

On the nature of change in Ni oxidation state in BaTiO₃–SrTiO₃ system

A. I. Lebedev* and I. A. Sluchinskaya

Physics Department, Moscow State University, Moscow, 119991, Russia

(Dated: October 28, 2016)

XAFS studies of Ni-doped Ba_{1-x}Sr_xTiO₃ solid solution reveal that the Ni oxidation state changes from 4 in SrTiO₃ to 2.5 in BaTiO₃ when varying x . This change is accompanied by a noticeable change in the interatomic Ni–O distances in the first shell. The first-principles calculations show that nickel creates an impurity band in the forbidden band gap of BaTiO₃ and SrTiO₃, which explains the appearance of intense absorption of Ni-doped samples in the visible region. The analysis of the electronic structure of doped crystals and calculations of the oxygen vacancy formation energy in them show that different oxidation states of Ni in SrTiO₃ and BaTiO₃ can be explained by different formation energies of the oxygen vacancies in these compounds.

DOI: 10.1080/00150193.2016.1198196

Keywords: doping, 3d impurities, oxidation state, electronic structure, barium titanate, strontium titanate

I. INTRODUCTION

Ferroelectric oxides with the perovskite structure are widely used in modern electronics for production of multilayer ceramic capacitors, various piezoelectric devices, and pyroelectric infrared detectors.^{1–3} Thin films of these materials are currently of great technological interest for tunable capacitors⁴ and dynamic random access memory (DRAM).^{1,5}

Barium titanate BaTiO₃, which is one of the end-member compound in the BaTiO₃–SrTiO₃ system, undergoes successive ferroelectric phase transitions from cubic $Pm3m$ to tetragonal $P4mm$ and further to orthorhombic $Amm2$ and rhombohedral $R3m$ phases with decreasing temperature. At 1460°C it undergoes a structural phase transition to the hexagonal $P6_3/mmc$ phase; the temperature of this transition can be controlled by doping BaTiO₃ with vacancies and various impurities.⁶ The other end-member compound, strontium titanate SrTiO₃, is an incipient ferroelectric, in which the softening of the TO mode is observed with decreasing temperature, but the samples remain paraelectric up to the lowest temperatures.⁷ At ~105 K SrTiO₃ undergoes an antiferrodistortive phase transition into the $I4/mcm$ phase. Barium titanate and strontium titanate form a continuous series of solid solutions Ba_{1-x}Sr_xTiO₃. When increasing the amount of SrTiO₃, the temperatures of all ferroelectric phase transitions are decreased and near $x = 0.8$ they merge into one phase transition.⁸ These solid solutions have been extensively studied because of their potential applications in various microelectronic devices.

Recently, perovskite ferroelectrics have attracted increasing attention because of their possible application in a new type of solar energy converters based on the bulk photovoltaic effect. Since oxide perovskites have a relatively large band gap (~3 eV), to match their absorption spectra to the solar radiation spectrum they can be doped with 3d-elements, which create so-called color centers.⁹ Theoretical studies¹⁰ have shown that the doping of a relative compound, PbTiO₃, by vacancy-compensated

divalent impurities with the d^8 electron configuration (Ni, Pd, Pt at the B site) can reduce the band gap to the levels optimal for effective energy conversion.

Strontium titanate doped with 3d-impurities (Mn, Co, Fe, and Ni) has recently been studied using XAFS spectroscopy.^{11–13} These studies have shown that Ni is one of the most promising dopants from the viewpoint of the effective sunlight absorption. The samples of Ni-doped strontium titanate were nearly black, the Ni ions were shown to substitute for Ti and, which was the most unusual, they were tetravalent. Unfortunately, SrTiO₃ is an incipient ferroelectric and its doping with nickel does not result in the appearance of ferroelectricity. This is why it is more interesting to study Ni-doped BaTiO₃.

Nickel is an important material for making electrical contacts to ferroelectric ceramics, and this is why the initial attention was paid to such questions as the Ni solubility in BaTiO₃ and its influence on the Curie temperature, dielectric constant, and other properties of BaTiO₃ as well as to the influence of nickel on the transition to the nonpolar $P6_3/mmc$ phase. It was shown that the incorporation of Ni decreases the transition temperature into the hexagonal phase, however, the solubility of nickel and its concentration needed for this transition strongly depend on the synthesis conditions, and the available data are very contradictory.^{6,14–17} It was found that Ni in BaTiO₃ acts as an acceptor,¹⁸ and the doping of barium titanate with nickel results in a decreasing of both the dielectric constant and the Curie temperature as well as in a smearing of the ferroelectric phase transition in BaTiO₃ with increasing Ni concentration.^{19–21} The transformation kinetics between the cubic and hexagonal phases in BaTiO₃ doped with different impurities was studied in Ref. 6. It was shown that nickel promotes the transition into the hexagonal phase, whereas the doping of BaTiO₃ with strontium, in contrast, prevents this transition. In Ref. 14 it was noticed that doping of BaTiO₃ with nickel changes its color to dark brown.

The information about the oxidation state and structural position of Ni in BaTiO₃ has been obtained mainly from EPR studies and is also very controversial. The lines observed in EPR spectra have been attributed to

the Ni^+ ions at the B sites,²² off-center Ni^+ ions at the A sites.²³ In Ref. 17, EPR studies of Ni-doped hexagonal BaTiO_3 have found Ni^{3+} ions that replaces Ti^{4+} in two different positions ($\text{Ti}(1)$ and $\text{Ti}(2)$); however, these centers can be associated with a maximum of 5% of the nominal amount of nickel, i.e. most of the Ni ions in the sample are in an EPR inactive state. The literature data on the oxidation state and structural position of nickel in SrTiO_3 have been summarized in our papers;^{12,13} no data on the subject for the $\text{Ba}_{1-x}\text{Sr}_x\text{TiO}_3$ solid solution was found.

One can see that, on the one hand, the optical properties of Ni-doped BaTiO_3 showing the strong absorption in the visible region in combination with its ferroelectric properties suggest that this material can be used in solar energy converters based on the bulk photovoltaic effect. On the other hand, despite the fact that $\text{BaTiO}_3(\text{Ni})$ has long been studied, the literature data on the Ni solubility, critical Ni concentration needed to transform BaTiO_3 into the hexagonal phase, its oxidation state, and structural position of Ni are very contradictory. Since the electronic transitions in Ni-related color centers are determined by the nickel oxidation state and the microscopic structure of these centers, in this work we used XAFS spectroscopy to determine the properties of the Ni impurity in the SrTiO_3 – BaTiO_3 system. The obtained data will be used to propose an adequate model for first-principles calculations, which will be used later to explain the observed optical properties of Ni-doped $\text{Ba}_{1-x}\text{Sr}_x\text{TiO}_3$ and to optimize the preparation conditions for obtaining material suitable for efficient solar energy converters.

II. SAMPLES, EXPERIMENTAL AND CALCULATION TECHNIQUES

Samples of SrTiO_3 , $\text{Ba}_{0.8}\text{Sr}_{0.2}\text{TiO}_3$, and BaTiO_3 doped with 0.5–3% Ni were prepared by the solid-state reaction method at 1500°C. The starting components were BaCO_3 , SrCO_3 , nanocrystalline TiO_2 obtained by hydrolysis of tetrapropylorthotitanate and dried at 500°C, and $\text{Ni}(\text{CH}_3\text{COO})_2 \cdot 4\text{H}_2\text{O}$. The components were weighed in required proportions, grinded in acetone, and annealed in air at 1100°C in alumina crucibles for 4–8 h. The resulting powder was grinded again and re-annealed in air at 1500°C for 2 h. In order to incorporate the impurity into the B site, the composition of the samples was intentionally deviated from stoichiometry toward the Ba excess. The phase composition of the samples was checked by X-ray method. The samples were single-phase and had cubic or hexagonal perovskite structures at 300 K. The synthesis of the NiTiO_3 and $\text{BaNiO}_{3-\delta}$ reference compounds was described in Ref. 13.

Measurements of X-ray absorption spectra in regions of the extended fine structure (EXAFS) and near-edge structure (XANES) were carried out at the KMC-2 station of the BESSY synchrotron radiation source at the

Ni K -edge (8.34 keV) in fluorescence mode at 300 K. The incident radiation was monochromatized using two-crystal $\text{Si}_{1-x}\text{Ge}_x(111)$ monochromator. The intensity of the radiation incident on the sample was measured using an ionization chamber, the intensity of the excited fluorescence was measured with a RÖNTEC X-flash energy-dispersive silicon detector with a working area of 10 mm².

EXAFS spectra were processed with the widely used IFEFFIT software package.²⁴ The EXAFS function was extracted from the experimental spectra using the ATHENA program, and its fitting to the theoretical curve calculated for a given structural model was performed using the ARTEMIS program. The amplitude and phase shifts for all paths of single and multiple scattering were calculated using the FEFF6 code.

Modeling of the geometry and electronic structure of Ni-doped BaTiO_3 and SrTiO_3 was performed within the first-principles density functional theory using the ABINIT software. The calculations were carried out on the 40-atom (SC) and 80-atom (FCC) supercells, in which one of Ti atoms was replaced by the Ni atom (the Ni concentration was 12.5 and 6.25%, respectively). The symmetry of supercells was cubic for both SrTiO_3 and BaTiO_3 . Since nickel has a partially filled d -shell, the PAW pseudopotentials²⁵ and LDA+ U approximation²⁶ were used in the calculations. The U and J parameters describing the Coulomb and exchange interaction within the d -shell were taken from the literature as $U = 5$ eV, $J = 0.9$ eV equal to typical values of these parameters for Ni; the changes by 20% of these parameters were shown to have a small influence on the results. The cut-off energy was 30 Ha, the integration over the Brillouin zone was carried out on a $4 \times 4 \times 4$ Monkhorst-Pack mesh. Relaxation of the lattice parameters and atomic positions in the supercells was stopped when the Hellmann-Feynman forces were below 1×10^{-5} Ha/Bohr.

The modeling on the 40-atom and 80-atom supercells without oxygen vacancies gave the results for the Ni^{4+} oxidation state. In order to change the oxidation state to Ni^{2+} , we used a trick²⁷ where two extra electrons were added to the system to change the filling of the d -shell. Although the system is not electrically neutral in this case, the tests have shown that the resulting density of states and the interatomic distances were very close to those calculated for the model in which the Ni^{2+} oxidation state was obtained by the addition of an oxygen vacancy at a distance of 5.8 Å from the Ni atom.

III. EXPERIMENTAL RESULTS

To determine the Ni oxidation state, the position of the absorption edge in XANES spectra of the samples was compared with those of the reference compounds. XANES spectra of SrTiO_3 , $\text{Ba}_{0.8}\text{Sr}_{0.2}\text{TiO}_3$, and BaTiO_3 samples doped with nickel and two reference compounds ($\text{BaNiO}_{3-\delta}$ and NiTiO_3) are shown in Fig. 1. It is seen that in $\text{BaTiO}_3(0.5\%\text{Ni})$ sample, the

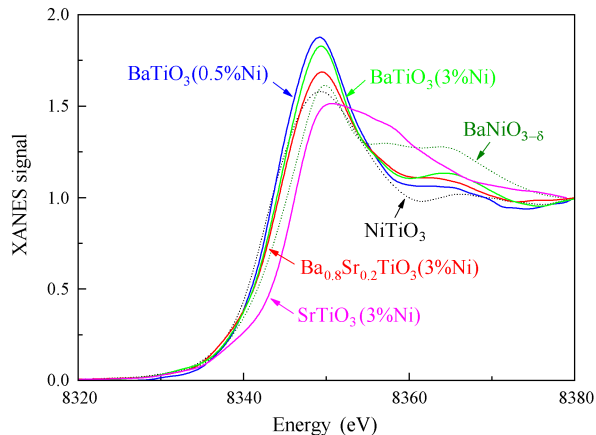


FIG. 1. (Color online) XANES spectra of four samples in the BaTiO₃–SrTiO₃ system and two reference compounds.

TABLE I. Local structure of investigated samples doped with 3% Ni.

Shell	R_i (Å)		
	SrTiO ₃	Ba _{0.8} Sr _{0.2} TiO ₃	BaTiO ₃ ^a
$R_{\text{Ni-O(I)}}$	1.914 ± 0.004	2.106 ± 0.008	2.069
$R_{\text{Ni-O(II)}}$		2.438 ± 0.021	
$R_{\text{Ni-Ba}}$	3.342 ± 0.006	3.428 ± 0.005	
$R_{\text{Ni-Ti}}$	3.877 ± 0.004	3.998 ± 0.005	

^aHexagonal structure.

absorption edge is closest to the absorption edge of the NiTiO₃ reference compound in which the oxidation state of nickel is 2+. In hexagonal BaTiO₃(3%Ni) and cubic Ba_{0.8}Sr_{0.2}TiO₃(3%Ni) samples, the positions of the absorption edge are almost the same and are shifted by 0.7 eV with respect to the absorption edge of NiTiO₃ toward the absorption edge of the BaNiO_{3-δ} reference compound, in which the oxidation state of nickel is 3.4+.²⁸ The absorption edge in Ni-doped SrTiO₃ sample is by 2.8 eV above the NiTiO₃ edge. If we assume that the Ni oxidation state in SrTiO₃ is 4+ (see the discussion in Ref. 13), we can conclude that the average oxidation state of Ni is ~ 2.3 in BaTiO₃(0.5%Ni) and ~ 2.5 in both BaTiO₃(3%Ni) and Ba_{0.8}Sr_{0.2}TiO₃(3%Ni). This means that the most of the nickel ions in the latter samples are in 2+ oxidation state, and only a fraction of them are in 3+ or 4+ states.

In order to determine the structural position of nickel in the samples, the EXAFS spectra were additionally analyzed. The best agreement between the calculated and experimental spectra for all samples was obtained in a model in which the Ni impurity atoms substitute for Ti⁴⁺ ions. In the case where Ni is in the 2+ oxidation state, the electrical neutrality of the sample is provided by a distant oxygen vacancy V_O . The interatomic distances in the first shell in investigated samples are given in Table 1.

It is seen that there is a significant difference in Ni–O distances in the first shell for different Ni oxidation states despite the fact that Ni atoms substitute for Ti atoms and are on-center in both SrTiO₃ and BaTiO₃. The obtained Ni–O distances are close to the sum of ionic radii of O²⁻ and Ni ions in corresponding oxidation states, so that the XANES and EXAFS data agree well.

IV. RESULTS OF FIRST-PRINCIPLES CALCULATIONS AND DISCUSSION

A surprising fact established in this work is a significant difference in the Ni oxidation state in two related compounds: it is about 2+ in both BaTiO₃ and Ba_{0.8}Sr_{0.2}TiO₃ and 4+ in SrTiO₃. This effect may result from the difference in the V_O formation energies and from the difference in relative positions of V_O donor levels and Ni acceptor levels in these compounds. In order to clarify the nature of this effect, we calculated the site-projected partial density of states (DOS) as well as the vacancy formation energy in nickel-doped BaTiO₃ and SrTiO₃.

The results of the DOS calculations are presented in Fig. 2. In the case of tetravalent nickel, the ground-state structure is diamagnetic ($S = 0$) for both BaTiO₃(Ni) and SrTiO₃(Ni). As follows from Fig. 2, an impurity band appears in the forbidden band gap of SrTiO₃ [Fig. 2(e)] and BaTiO₃ [Fig. 2(b)]. In both compounds, the band is slightly shifted toward the conduction band, but in SrTiO₃ it is located by 0.15–0.2 eV higher than in BaTiO₃. The comparison of DOS of doped [Fig. 2(b,e)] and undoped [Fig. 2(a,d)] compounds shows that the doping slightly increases the band gap of the samples (by 82 meV for BaTiO₃ and by 91 meV for SrTiO₃ upon adding of 6.25% of Ni). It also increases the width of the valence band. The Fermi level in doped crystals is located in the forbidden gap between the impurity and the valence bands (dashed lines in the figure). The obtained results disagree with the conclusion of Ref. 10 about decreasing of the energy band gap upon Ni doping. The width of the impurity band is ~ 0.11 eV in SrTiO₃ and BaTiO₃ doped with 6.25% Ni and increases to 1.1–1.7 eV when doubling the impurity concentration.

For divalent nickel, the ground-state structure is paramagnetic ($S = 1$) in both BaTiO₃(Ni) and SrTiO₃(Ni). Because of the appearance of magnetic moment, the energy position of the Ni spin-up and spin-down 3d states is different: the spin-up states are pushed down below the Fermi level, and the spin-down states are shifted up and are located in the conduction band. In both compounds, the impurity band is shifted toward the valence band, and the Fermi level is located between the fully occupied spin-up states and the conduction band edge [Fig. 2(c) and 2(f)]. The energy splitting of the O 2p spin-up and spin-down states indicates a partial magnetization of the oxygen ions located in the vicinity of the paramagnetic Ni²⁺ centers.

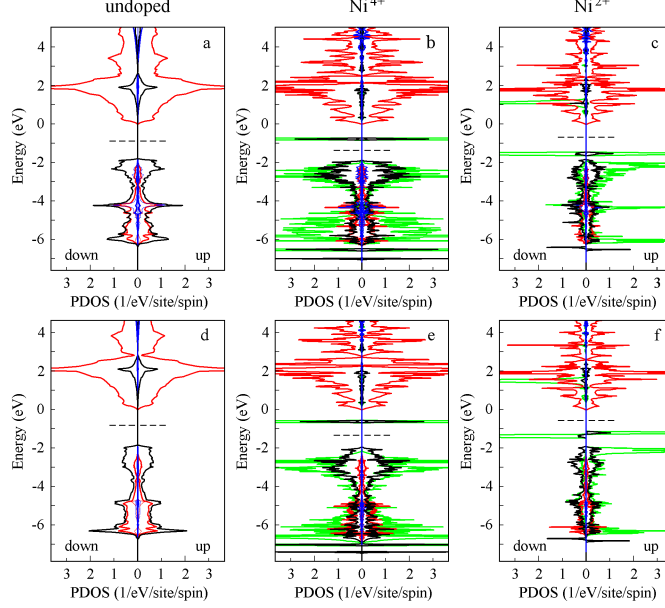


FIG. 2. (Color online) Site-projected partial density of states for undoped and Ni-doped samples of (a–c) BaTiO_3 and (d–f) SrTiO_3 . Ti 3d states are shown by red, Ni 3d states are shown by green, O 2p states are shown by black, and Ba 5d (Sr 4d) states are shown by blue. The Fermi levels are depicted by dashed lines.

The formation energy of the oxygen vacancy in Ni-doped samples was calculated as the difference between the total energy of the structure containing the Ni^{4+} ion and the sum of the energy of the structure containing the $\text{Ni}^{2+}-\text{V}_\text{O}$ complex and a half of the energy of the O_2 molecule in the triplet state. It was 3.14 eV for $\text{SrTiO}_3(\text{Ni})$ and 2.69 eV for $\text{BaTiO}_3(\text{Ni})$.

We believe that the difference in the Ni behavior in SrTiO_3 and BaTiO_3 is due to the difference in V_O formation energies in these materials. Indeed, previous calculations of the energy levels of the oxygen vacancies^{29,30} have shown that these levels are located in the upper half of the forbidden gap and so are higher than the Ni acceptor levels. Therefore, the filling of the Ni^{4+} levels by electrons from the oxygen vacancies is energetically favorable in both materials. On the other hand, our calculations show that the formation energy of the oxygen vacancy in Ni-doped BaTiO_3 is notably lower than in Ni-doped SrTiO_3 . So, we can conclude that the observed difference is associated with different formation energies of the oxygen vacancy in these materials.

The proposed model can also qualitatively explain the effect of the impurity concentration on the average oxidation state of Ni in doped samples. At low doping level, the Ni impurity band is narrow, and its occupation by electrons is determined by the relative energy positions of Ni and V_O levels. When the impurity concentration increases, the energy bands formed from the Ni and V_O levels become broad. Because of the overlapping of these bands, the filling of the Ni impurity band asymptotically approaches that corresponding to the 3+ oxidation state, in agreement with experiment.

It should be noted that our calculations of the electronic structure of a number of nickel compounds have shown that the Ni–O interatomic distance is mainly determined by the magnetic state of Ni rather than by its oxidation state. In particular, it appeared that the $\text{Ni}^{2+}-\text{V}_\text{O}$ complex with the neighboring oxygen vacancy considered in Ref. 10 is diamagnetic and is characterized by $4 \times 1.870 + 1 \times 2.144$ Å Ni–O distances, which are very different from the distances obtained from the EXAFS data analysis. So, only the paramagnetic Ni complexes with distant vacancies can explain the Ni–O distance observed in experiment.

To check the proposed model, in future it would be interesting to study the evolution of the Ni oxidation state upon change of the composition x in the whole $\text{BaTiO}_3-\text{SrTiO}_3$ system. The measurements of magnetic susceptibility and determination of the spin concentration in the samples can be also useful to check this model.

The location of the Ni impurity band near the middle of the forbidden gap of SrTiO_3 and BaTiO_3 can explain the strong absorption observed in all studied samples by electronic transitions between the impurity band and the valence or conduction bands.

V. CONCLUSIONS

XAFS studies of Ni-doped $\text{Ba}_{1-x}\text{Sr}_x\text{TiO}_3$ solid solution have revealed that the Ni oxidation state changes from 4 in SrTiO_3 to 2.5 in BaTiO_3 when varying x . This change is accompanied by a noticeable change in the interatomic Ni–O distances in the first shell. The

first-principles calculations showed that nickel creates an impurity band in the forbidden band gap of BaTiO₃ and SrTiO₃, which explains the appearance of intense absorption of Ni-doped samples in the visible region. The analysis of the electronic structure of doped crystals and calculations of the oxygen vacancy formation energy in them showed that different oxidation states of Ni in SrTiO₃ and BaTiO₃ can be explained by different formation en-

ergies of the oxygen vacancies in these compounds.

ACKNOWLEDGMENTS

This work was supported by Russian Foundation for Basic Research, grant No. 13-02-00724. The authors would like to thank the BESSY staff for continuous support of our experiments.

-
- * swan@scon155.phys.msu.ru
- ¹ K. Uchino, *Ferroelectric Devices 2nd Edition* (CRC Press, 2009).
 - ² C. Pithan, D. Hennings, and R. Waser, *Int. J. Appl. Ceram. Technol.* **2**, 1 (2005).
 - ³ S. G. Porter, *Ferroelectrics* **33**, 193 (1981).
 - ⁴ A. Tagantsev, V. Sherman, K. Astafiev, J. Venkatesh, and N. Setter, *J. Electroceram.* **11**, 5 (2003).
 - ⁵ J. F. Scott, *Annu. Rev. Mater. Sci.* **28**, 79 (1998).
 - ⁶ R. M. Glaister and H. F. Kay, *Proc. Phys. Soc.* **76**, 763 (1960).
 - ⁷ K. A. Müller and H. Burkard, *Phys. Rev. B* **19**, 3593 (1979).
 - ⁸ V. V. Lemanov, E. P. Smirnova, P. P. Syrnikov, and E. A. Tarakanov, *Phys. Rev. B* **54**, 3151 (1996).
 - ⁹ G. Blasse, P. H. M. de Korte, and A. Mackor, *J. Inorg. Nucl. Chem.* **43**, 1499 (1981).
 - ¹⁰ G. Y. Gou, J. W. Bennett, H. Takenaka, and A. M. Rappe, *Phys. Rev. B* **83**, 205115 (2011).
 - ¹¹ A. I. Lebedev, I. A. Sluchinskaya, A. Erko, and V. F. Kozlovskii, *JETP Lett.* **89**, 457 (2009).
 - ¹² I. A. Sluchinskaya, A. I. Lebedev, and A. Erko, *J. Adv. Dielectrics* **3**, 1350031 (2013).
 - ¹³ I. A. Sluchinskaya, A. I. Lebedev, and A. Erko, *Phys. Solid State* **56**, 449 (2014).
 - ¹⁴ Y. C. Huang and W. H. Tuan, *Mater. Chem. Phys.* **105**, 320 (2007).
 - ¹⁵ F. Boujelben, F. Bahri, C. Boudaya, A. Maalej, H. Khemakhem, A. Simon, and M. Maglione, *J. Alloys Comp.* **481**, 559 (2009).
 - ¹⁶ S. K. Das, R. N. Mishra, and B. K. Roul, *Solid State Commun.* **191**, 19 (2014).
 - ¹⁷ R. Böttcher, H. T. Langhammer, and T. Müller, *J. Phys.: Condens. Matter* **23**, 115903 (2011).
 - ¹⁸ E. Duverger, B. Jannot, M. Maglione, and M. Jannin, *Solid State Ionics* **73**, 139 (1994).
 - ¹⁹ Y.-C. Huang and W.-H. Tuan, *J. Electroceram.* **18**, 183 (2007).
 - ²⁰ J. Q. Huang, P. Y. Du, W. J. Weng, and G. R. Han, *J. Electroceram.* **21**, 394 (2008).
 - ²¹ Y. Kumar, M. A. Mohiddon, A. Srivastava, and K. L. Yadav, *Ind. J. Eng. Mater. Sci.* **16**, 390 (2009).
 - ²² T. W. Kool, S. Lenjer, and O. F. Schirmer, *J. Phys.: Condens. Matter* **19**, 496214 (2007).
 - ²³ S. Lenjer, R. Scharfschwerdt, T. W. Kool, and O. F. Schirmer, *Solid State Commun.* **116**, 133 (2000).
 - ²⁴ Ifeffit project home page, <http://cars9.uchicago.edu/ifeffit/>.
 - ²⁵ K. F. Garrity, J. W. Bennett, K. M. Rabe, and D. Vanderbilt, *Comput. Mater. Sci.* **81**, 446 (2014).
 - ²⁶ V. I. Anisimov, F. Aryasetiawan, and A. I. Lichtenstain, *J. Phys.: Condens. Matter* **9**, 767 (1997).
 - ²⁷ A. V. Postnikov, A. I. Poteryaev, and G. Borstel, *Ferroelectrics* **206**, 69 (1998).
 - ²⁸ The Ni oxidation state in this sample was determined in Ref. 13.
 - ²⁹ R. A. Evarestov, E. A. Kotomin, and Y. F. Zhukovskii, *Int. J. Quant. Chem.* **106**, 2173 (2006).
 - ³⁰ M. Choi, F. Oba, and I. Tanaka, *Appl. Phys. Lett.* **98**, 172901 (2011).